PFC/JA-95-42

X-ray and VUV Observations of Mo^{23+} - Mo^{33+} Brightness Profiles from Alcator C-Mod Plasmas

J.E. Rice, J.L. Terry, K.B. Fournier[1],
M.A. Graf, M. Finkenthal[2], M.J. May[2],
E.S. Marmar, W.H. Goldstein[1], A.E. Hubbard,

November, 1995

[1]Lawrence Livermore National Laboratory, Livermore, CA.
[2]Johns Hopkins University, Baltimore, MD.

Submitted to Journal of Physics B.

This work was supported by the U. S. Department of Energy Contract No. DE-AC02-78ET51013. Reproduction, translation, publication, use and disposal, in whole or in part by or for the United States government is permitted.

X-ray and VUV Observations of Mo^{23+} - Mo^{33+} Brightness Profiles from Alcator C-Mod Plasmas

J. E. Rice, J. L. Terry, K. B. Fournier[+], M. A. Graf, M. Finkenthal[*],
M. J. May[*], E. S. Marmar, W. H. Goldstein[+] and A.E. Hubbard
Plasma Fusion Center, MIT
Cambridge, MA 02139-4307

[+] *Lawrence Livermore National Laboratory, Livermore, CA 94550*
[*] *Johns Hopkins University, Baltimore, MD 21218*

Abstract

Brightness profiles of X-ray and VUV lines from eight molybdenum charge states between Mo^{23+} and Mo^{33+} have been measured in Alcator C-Mod plasmas. These spatial profiles agree very well with those predicted by a model which includes ionization, recombination, excitation and transport. Comparison with the profiles of many different charge states provides severe constraints upon the rates used in the model. The charge state density profiles are calculated using measured impurity transport coefficients, measured electron density and temperature profiles and newly calculated ionization and recombination rate coefficients. These new rate coefficients include direct collisional ionization, excitation-autoionization, dielectronic and radiative recombination. Excitation-autoionization is shown to be an important process, since the excellent agreement between the measurements and predictions is obtained only with its inclusion. Fits to newly calculated excitation rate coefficients for the transitions are also presented.

Introduction

There is renewed interest in the use of high Z plasma facing components in the next generation of magnetically-confined fusion devices, so the tradition of the study of highly ionized molybdenum (Z = 42) continues. The primary concern is that radiated power from molybdenum ions in a burning core will be detrimental to energy confinement and to ignited performance. In particular, upper limits on the fraction of high Z ions in the core of an ignited plasma have been calculated[1]. For molybdenum this upper limit concentration is $\sim 10^{-3}$, while for tungsten it is $\sim 10^{-4}$. Thus, the ability to determine accurately concentrations and radiated power fractions of high Z elements is important if these elements are present in future tokamak fusion reactors. This capability is already desired in the present generation of tokamaks. The major plasma facing components in the Alcator C-Mod Tokamak[2] are molybdenum tiles. The FTU tokamak has a molybdenum toroidal belt limiter[3]. The TEXTOR tokamak has experimented with molybdenum and with tungsten limiters[4], and Asdex-Upgrade has investigated the use of tungsten as a divertor target material[5].

To determine the concentrations and radiated power fractions from measurements of line brightnesses, the charge state balance and line excitation rates must be known. For determining charge state balance, knowledge of the important ionization and recombination processes is necessary, as is quantitative evaluation of the rates, and knowledge both of the impurity transport and the electron density and temperature profiles. For the relatively low density ($n_e \lesssim 5 \times 10^{21} m^{-3}$) conditions obtained in tokamak plasmas, the ionization balance of impurity ions is determined by collisions with electrons, radiative and dielectronic recombination, and transport. A collisional-radiative model is used to predict line emission. The important ionization processes are the well known "direct ionization" and excitation-autoionization (EA). The importance of EA as an ionization process has been noted previously[6], where rate coefficients for simpler ions (e.g. Na-like and Li-like) have been calculated for lower Z elements. EA cross-sections for the simpler ions of heavier

elements, including Mo, have also been calculated[7]. However, until recently[8], there was no *comprehensive* set of excitation-autoionization and dielectronic recombination (DR) rate coefficients for the relevant (Mo^{23+} - Mo^{33+}) charge states of molybdenum. (Fully relativistic *ab initio* calculations of DR for Ne-like and F-like Mo are available[9].) It is this comprehensive set of accurate atomic physics data which is necessary for the precise modelling of molybdenum in a tokamak plasma.

It has been shown that the EA rate coeffiecients[8] used in this paper can dominate (by a factor of 3) those of direct collisional ionization for some molybdenum charge states[10]. When the rates[8] for DR in Mo^{23+} through Mo^{33+} are compared with radiative recombination, it seen that DR is the dominant recombination process. To determine the power radiated from each ionization state, it is necessary to identify the important radiative transitions and their excitation (population) mechanisms. This paper compares measured and calculated brightness profiles of selected lines from eight molybdenum charge states. The agreement between experiment and prediction over the profiles of many ionization states requires that the ionization and excitation rate coefficients be accurate and that impurity transport be well characterized. Finally, the confidence in the ionization balance and excitation modeling, which this comparison brings, allows accurate determination of the molybdenum concentration from measured line brightnesses.

The organization of this paper is as follows: First, an overview of Alcator C-Mod and the x-ray and VUV spectrometer systems is presented. There follows the calculation of charge state distributions from MIST[11], the transport code used to model the molybdenum impurity. This will show the importance of excitation-autoionization as an ionization process for many of the charge states. Next are shown the newly calculated excitation rate coefficients for several of the observed x-ray and VUV lines, analytic approximations to the rate coefficients, and a comparison of measured and calculated central chord line brightnesses for several transitions in Mo^{32+}. The main body of this paper compares the measured and predicted radial brightness profiles of VUV and x-ray lines from eight molybdenum charge states (Mo^{23+} - Mo^{25+}, Mo^{29+} - Mo^{33+}), and the calculation of absolute molybde-

num densities in the plasma.

Alcator C-Mod and Instrumental Descriptions

Alcator C-Mod is a compact (a = 0.225 m, R = 0.665 m), high magnetic field diverted tokamak[2], with the capability of 4 MW of auxiliary heating power at 80 MHz. The parameter ranges achieved for the device to date are 2.5 T $\leq B_T \leq$ 6.5 T, .3 MA $\leq I_P \leq$ 1.2 MA, .2 x $10^{20}m^{-3} \leq n_e \leq$ 2.5 x $10^{20}m^{-3}$, 1.0 $\leq \kappa \leq$ 1.8 and .7 keV $\leq T_{e0} \leq$ 4.5 keV. Most of the plasma facing components, in particular the divertor and inner wall, are made of molybdenum.

The x-ray spectra presented here were recorded by a five chord, independently spatially scannable, high resolution x-ray spectrometer array[12]. Each von Hamos type spectrometer consists of a variable entrance slit, a quartz crystal (2d = 6.687 Å) and a position sensitive proportional counter detector. Each spectrometer has a resolving power of 4000, a 2 cm spatial resolution and a wavelength range of 2.8 to 4.1 Å. Spectra are typically collected every 50 ms during a discharge, with 120 mÅ covered at any one wavelength setting. A nominal value of the spectrometer luminosity function is 7 x 10^{-13} m^2sr, calculated from the crystal reflectivity, spectrometer geometry, detector sensitivity and Be window transmission.

VUV spectra were obtained with a 2.2 m, absolute intensity calibrated, grazing incidence spectrograph[13], which utilizes a micro-channel plate detector coupled to a 1024 element, self-scanning (Reticon©[14]) linear array. Spectral resolution of the instrument is typically .5 to 1 Å. The line-of-sight can be scanned vertically on a shot-to-shot basis, with a spatial resolution at the plasma of 1.5 cm . The 1^{st} order wavelength range of the system is from 60 to 1100 Å, with ~50 Å covered at one time. Spectra can be collected in as little as 0.5 ms, although for this work, typical integration times were 2 ms.

The scanning ranges of the two systems are shown in Fig. 1, superimposed on a magnetic flux surface reconstruction from EFIT[15]. In order to display the chord

brightness profiles and to compare them with model predictions, it is assumed that the emissivity is a flux function. Thus the profiles are plotted versus the minor radius of a point determined as follows: first, the flux surface to which the viewing chord is tangent is found, then this point is mapped along the flux surface to the plasma midplane. The viewing chord "ρ" is the minor radius (measured from the magnetic axis) of this mapped point. This is illustrated schematically in Fig. 1 by the thick curved lines running from the viewing chords to the midplane. ρ for the VUV line of sight is 18.2 cm, the difference between the asterisk at .866 m and the magnetic axis at R=.684 m (the + sign). ρ for the x-ray line of sight, shown by the diamond, is 9.7 cm.

A second VUV instrument has been used to measure the shot-to-shot variation of molybdenum emission which occurred while the VUV spectrograph was being scanned in space. A Multi-Layer-Mirror-based (MLM) polychromator[16], looking approximately through the midplane, monitored the Na-like Mo^{31+} line emission at 128 Å with 7 Å (FWHM) resolution, and the Mo^{25+} emission and quasi-continuum at 76 Å with 3 Å resolution.

The Charge State Distributions

The charge state distribution for molybdenum can be calculated from the MIST[11] impurity transport code, incorporating the new excitation-autoionization and dielectronic recombination rates from Ref. (8), using measured electron temperature and density profiles, and impurity transport coefficients. As an example for calculating charge state density profiles, consider a typical ICRF heated discharge[17], the time evolution of which is depicted in Fig. 2. During the current flat top of .8 MA, the RF power was around 1 MW, the central electron temperature was 2200 eV and the central electron density was 1.6 x $10^{20}m^{-3}$. Also shown are the time histories of VUV and x-ray emission from central molybdenum charge states, Mo^{31+} and Mo^{32+}, and Z_{eff} from the visible continuum. There is a deliberate molybde-

num injection at .4 s from the laser blow-off injection system. For this particular 5.4T, deuterium discharge, the electron temperature and density profiles, obtained from the ECE[18] and laser interferometer[19] diagnostics, are shown in Fig. 3, at .4 and .65 s. Impurity transport is modeled as

$$\Gamma_z = -D\nabla n_z + V_0\, n_z\, \frac{r}{a}, \qquad (1)$$

where D = 0.5 m^2/sec and V_0 = 2 m/sec, values determined from other impurity injection experiments[20], and consistent with the ~20 ms exponential decay time of the VUV signal in Fig. 2. Shown in Fig. 4a are the fractional abundances of molybdenum charge states as a function of minor radius in the plasma, calculated following Eq.(1) in Ref (21), using the new ionization and recombination rates, and the profiles from Fig. 3 at .65 seconds. The new ionization rate coefficients include contributions from direct ionization, calculated using the formulas found in Ref. 22, and for EA as found in Ref. 8. Ne-like Mo^{32+} is the dominant state over most of the interior plasma and the neighboring charge states are all present in appreciable quantities. The Na-like Mo^{31+} profile peaks around 7 cm. and the Cl-like Mo^{25+} profile peaks at 13.8 cm. Shown for comparison in Fig. 4b are the charge state profiles calculated using older ionization[23] rates with no EA and recombination[24–26] rates using a semi-empirical form for DR. There is a striking difference in the core charge state distribution, largely due to the effects of the more accurate calculation of direct collisional ionization and inclusion of excitation-autoionization. The central fractional abundance of Mo^{32+} is a factor of 3 lower in Fig. 4b than in Fig. 4a, and the profile shapes have all changed. The Mo^{31+} state is now centrally peaked and the peak in Mo^{25+} is at 12.8 cm. These differences can strongly affect conclusions about molybdenum densities in the plasma from various charge states. In order to calculate line emissivities, the excitation rates are also needed.

The Observed Spectral Lines

The x-ray and VUV lines used in this paper for comparison with the model profile predictions are listed in Table I. They are from eight charge states between F-like Mo^{33+} and K-like Mo^{23+}. For the electron temperatures obtained in Alcator C-Mod, these states reside in the central two-thirds of the plasma. Representative spectra including these lines, taken along central viewing chords, are shown in Figs. 5a-8a. Fig. 5a displays the x-ray spectrum between 3.7 and 3.8 Å, taken during the ICRF heated period of the discharge. Observed are 2p-4d transitions in charge states between Mo^{30+} and Mo^{33+}. This spectrum is dominated by the $2p_{\frac{3}{2}}$-$4d_{\frac{5}{2}}$ transition in Mo^{32+} at 3.7398 Å[27]. Other strong transitions in the spectral range from 3.6 to 3.7 Å from these centrally located charge states, for a similar shot, are shown in Fig. 6a. This spectrum is dominated by the $2p_{\frac{1}{2}}$-$4d_{\frac{3}{2}}$ transition in the Ne-like state at 3.6261 Å[27]. In Fig. 7a is the VUV spectrum between 115 and 130 Å, taken during the deliberate molybdenum injection into a discharge similar to that shown in Fig. 2. It shows the strong 3s-3p transitions from the charge states Mo^{31+} and Mo^{30+}, and a 3p-3d transition from Mo^{29+}. The VUV central chord spectrum between 65 and 85 Å is shown in Figs. 8a and 8b. Most of the strong features are from the Mo^{23+} through Mo^{25+} charge states and are emitted from regions near r/a$\sim$0.6. The wavelengths of some of these lines shown in Figs 5-8 and listed in Table I have been previously measured in TFR[28], ST[29], DITE[30], PLT[31,32], TEXT[33–38], Alcator C-Mod[27], exploding wires[39] and/or laser produced plasmas[40,33–38].

Excitation Rates

Electron impact excitation rates for these and other lines have been generated using the HULLAC suite of codes. HULLAC includes the parametric potential code RELAC [41,42] which calculates the *ab initio* relativistic wavefunctions, energy levels, and radiative transition probabilities. Also included is the CROSS suite of codes[43] which computes the electron impact excitation rate coefficients in the distorted wave approximation. The calculated coefficients allow for a self-consistent determination

of the steady-state populations of all levels at a given temperature and density in a collisional-radiative model. For Ne-like through Mg-like molybdenum, the dominant steady-state population is in a single (ground) state. As an example, shown in Fig. 9 are excitation rate coefficients as a function of electron temperature for the two 2p-nd series of Mo^{32+} with $4 \leq n \leq 12$. The solid lines are for the $2p_{\frac{3}{2}}$-$nd_{\frac{5}{2}}$ series and the dotted lines are for the $2p_{\frac{1}{2}}$-$nd_{\frac{3}{2}}$ series.

For ease of use in modeling codes, fits to the excitation rate coefficients have been made using the formalism in Ref.(44). The excitation rate coefficient is fit to the function

$$Q = \frac{1.58 \times 10^{-5} f_{ij}\ g\ e^{(-E_{ij}/T_e)}}{E_{ij}\sqrt{T_e}}\ cm^3/s, \qquad (2)$$

where f_{ij} is the oscillator strength, T_e is the electron temperature (eV), E_{ij} is the transition energy (eV) and g is the average Gaunt factor, given by

$$g = A + (By - Cy^2 + D)\ e^y\ E_1(y) + Cy \qquad (3)$$

where $y = E_{ij}/T_e$ and $E_1(y)$ is the exponential integral. A, B, C and D are numerical constants. For the appropriate transitions, the calculated excitation rate coefficients of the CROSS codes are fit by taking C = 0 and D = .28, as recommended in Ref. 44, and varying the parameters A and B. The fits for A and B, along with the wavelengths and oscillator strengths for the transitions of Table I and the high n series of Mo^{32+} are given in Table II. Using these values for A and B gives analytic approximations to the excitation rate coefficients which are within 1% for the x-ray lines and 3% for the VUV lines compared to the calculated values.

Given electron density and temperature profiles, charge state density profiles, excitation rates and viewing lines of sight, emissivity profiles and chordal brightnesses may be calculated. As a test of the relative accuracy of the excitation rates for the $\Delta n \geq 2$ x-ray transitions in Mo^{32+}, the measured and predicted brightnesses are compared. Central chord brightnesses of the $2p_{\frac{3}{2}}$-$nd_{\frac{5}{2}}$ and $2p_{\frac{1}{2}}$-$nd_{\frac{3}{2}}$ series in Mo^{32+} were observed from a series of similar 460 kA, 5.2 T deuterium discharges with $n_{e0} = 7.7 \times 10^{19} m^{-3}$ and $T_{e0} = 2300$ eV, and are shown as symbols in Fig. 10.

The calculated brightnesses as a function of n are shown as the curves in Fig. 10, normalized at only one point (the $2p_{\frac{3}{2}}$-$4d_{\frac{5}{2}}$ brightness) and the agreement is quite good. Note that the brightnesses do not follow a smooth n^{-3} dependence due to the configuration interaction between certain levels[45,27] which, in particular, leads to an enhancement of the $2p_{\frac{3}{2}}$-$7d_{\frac{5}{2}}$ line at the expense of the $2p_{\frac{1}{2}}$-$6d_{\frac{3}{2}}$ line. This is also reflected in the excitation rate coefficients shown in Fig 9. There are no data points for the $2p_{\frac{1}{2}}$-$8d_{\frac{3}{2}}$ and $2p_{\frac{1}{2}}$-$9d_{\frac{3}{2}}$ transitions because these are not resolved in wavelength from the $2p_{\frac{3}{2}}$-$11d_{\frac{5}{2}}$ and $2p_{\frac{3}{2}}$-$14d_{\frac{5}{2}}$ transitions[27], respectively.

Molybdenum Densities and Brightness Profiles

Since the upper states of almost all of these transitions are populated primarily by direct electron impact excitation, the brightnesses of the VUV and x-ray lines are related to the absolute molybdenum density in the plasma as

$$n_{Mo} = \frac{B}{(\int n_e(\psi)\, f_{Mo}(\psi)\, Q_{eff}(T_e(\psi))\, dl)\, \epsilon} \qquad (4)$$

where B is the measured brightness of a particular line of interest, n_e and T_e are measured electron density and temperature profiles (as in Fig. 3), f_{Mo} is the normalized profile of the appropriate charge state (calculated from MIST, as in Fig. 4), Q_{eff} is the "effective" excitation rate coefficient (Eq. 2) of the line (where "effective" includes the fact that for some charge states (Mo $^{23+,24+,25+,29+}$) there is a significant population not in the ground state), ϵ is the branching ratio for the transition, and ψ is the flux surface coordinate. The use of ψ implies the assumption that the dependent quantity is constant over a flux surface. The integral is performed along the observation line of sight. The central molybdenum density has been determined from three separate diagnostics for the discharge shown in Fig. 2, during the molybdenum injection at .4 seconds. From the increase in the Mo^{31+} 128 Å line emission, a central molybdenum density of 6.9 x $10^{16}m^{-3}$ at the injection peak is determined. From the increase of the Mo^{32+} line at 3.7398 Å, a density of 2.9 x $10^{16}m^{-3}$ is obtained in the same fashion, in reasonable agreement. There is

a 30% uncertainty in the sensitivity of the VUV observations at this wavelength, and the luminosity function of the x-ray spectrometers is only accurate to within a factor of two. The molybdenum density may also be obtained from the increase in Z_{eff} due to the injection. From Fig. 2, the increase in Z_{eff} was .25, which gives a molybdenum density of

$$n_{Mo} = \frac{\Delta Z_{eff}\, n_e}{(Z_{Mo})(Z_{Mo}-1)} = 3.3 \times 10^{16} m^{-3},$$

using Z_{Mo}=32, in good agreement with the densities determined from line brightnesses.

Alternatively, given the total molybdenum density in the plasma, brightnesses of individual lines may be calculated from Eq. 4. From the calculated line brightnesses, synthetic spectra may be generated, using instrumental and Doppler widths, and measured or theoretical wavelengths. In this way the central chord Mo spectra in these VUV and x-ray spectral regions have been generated using the MIST code and the new atomic physics rates. The predicted spectra are shown in Figures 5b, 6b, 7b and 8c. The wavelengths used for the prediction are given in Table I for the VUV lines and taken from Ref. 27 for the x-ray lines. As shown, the relative intensities of the lines from various charge states are in good agreement with the observations, especially in Figs 5-7. In Figure 8, there are differences of ~50% in the intensity of the Mo^{25+} line at 76.6 Å, in the relative intensities of the Mo^{23+} lines at 71-72 Å, and in the features at 75.7 and 78.5 Å. These clearly resolved lines are seen on top of a "quasi-continuum" of emission. In order to measure the line brightnesses, this "continuum", assumed to be smooth function of wavelength, has been subtracted, with the result shown in Fig 8b. This is to be compared with the Mo spectrum predicted for these charge states, shown in Fig 8c. Although the agreement is within a factor of 2, it is not as good as that found for emission from higher charge states (see Figs 5-7). Work in progress indicates that the "quasi-continuum" is actually the sum of many unresolved lines from charge states lower than Mo^{23+} and is not as smooth as assumed in the subtraction. Thus the actual

shape of the unresolved emission influences the determination of the Mo^{23+}-Mo^{25+} line brightnesses and may lead to the observed disagreement.

The spectra from Figs. 5a-8a were from central chord observations. The VUV and x-ray spectrometers are scannable in the vertical plane, to obtain spectra along different radii. Shown in Figs. 5c-7c are spectra from the same wavelength ranges as Figs. 5a-7a, respectively, for similar discharges, but from non-central lines of sight. In Fig. 5c is a spectrum taken along a line of sight which is tangent to the flux surface that is 6.5 cm (i.e. ρ=6.5 cm) outside the plasma center on the plasma midplane. The overall intensities are greatly reduced from Fig. 5a, the Mo^{31+} line has grown relative to the Mo^{32+} transition, and the Mo^{33+} line has nearly disappeared. Shown in Fig. 6c is a spectrum at 6.7 cm for the same spectral range as Fig. 6a . The Na-like Mo^{31+} line has increased and the F-like Mo^{33+} line has decreased compared to the Ne-like Mo^{32+} line. The intensities of all the lines are greatly diminished compared to the central chord spectrum. Shown in Fig. 7c is a VUV spectrum obtained along a line of sight with ρ=7.4 cm. The overall intensity of the Na-like line has decreased a factor of three or so, much less than in the case of the x-ray transitions. This is a result of the strong temperature dependence in the excitation rate coefficients of the x-ray lines. The Al-like Mo^{29+} line has increased relative to the stronger Mg-like and Na-like lines.

Complete spatial brightness profiles have been obtained by scanning the spectrometer systems on a shot by shot basis during a sequence of similar discharges. For the x-ray brightness profiles, one spectrometer was maintained viewing the plasma center to serve as a monitor of the molybdenum brightness, in case there was any variation shot to shot. For the VUV profiles, the VUV MLM (measuring the emissions at 128 Å and 76 Å) provided the normalization while the spectrograph was being scanned. The shot-to-shot variation in the 128 Å line was $\pm$30% over the molybdenum injections at 0.4 s. Radial brightness profiles of the five most intense x-ray lines (3.6149, 3.6261, 3.6710, 3.7398 and 3.7857 Å), obtained during the 1 MW portion of the RF pulse in several similar shots, are shown in Fig. 11. The

Mo^{32+} profiles (Xs and plus signs) dominate over the inner half of the plasma. The Mo^{31+} profile shapes (squares and diamonds) are broader, and the Mo^{33+} profile (asterisks) is more narrow than the Mo^{32+} profiles. Also shown in the figure are the calculated brightness profiles (curves) for the five lines, and the agreement is excellent. All of the profile shapes and the relative intensities are well matched by the calculations. This agreement indicates that the combination of the electron temperature and density profiles, the transport coefficients and the excitation, ionization and recombination rates is well characterized for these ionization states over the inner 10 cm. In this region the electron temperature and density profiles and impurity transport coefficients are independently measured and well known. (Fig.3) The excitation rates, at least for Mo^{32+}, agree with the observations, as shown in Fig. 10. Thus the match in Fig. 11 is taken as evidence in support of the charge state profiles shown in Fig. 4a. The brightness profiles calculated from the charge state profiles of Fig. 4b (i.e. those without EA) are shown in Fig. 12, along with the measured profiles. Both the profile shapes and the relative intensities do not represent the data, demonstrating the importance of excitation-autoionization in the overall ionization rate and the sensitivity of this comparison.

VUV brightness profiles have been obtained in the same fashion during the molybdenum injection at .4 seconds (Fig. 2). Shown in Fig. 13 are the comparisons between the measured (points) and predicted profiles (lines) of Mo^{31+}, Mo^{30+}, Mo^{29+}, Mo^{25+}, Mo^{24+} and Mo^{23+} line brightnesses. There is a single normalization, in this case made to a by-eye match to the near-central chord brightnesses of the Mo^{31+} line (although a normalization to the Mo^{30+} line would yield an equally good fit). The agreement is quite good, especially for the near-central chord brightnesses, except that the four Mo^{23+} lines around 71 Å are predicted to be ~50% lower (this is also evident in Fig 8). There are some systematic differences in all the profiles for $\rho \gtrsim 9$ cm. The observed profiles are somewhat narrower than predicted, and Mo^{25+} and Mo^{24+} profiles peak inside of the predictions. It is unclear what is responsible for these differences; there are uncertainties in the electron temperature profiles in the outer regions of the plasma, and the impurity diffusion coefficient

has been taken to be spatially constant, which may not be the case. Both of these effects can contribute to uncertainties in the calculated brightness profiles in the outer regions. The differences between the measured profiles and those calculated without inclusion of the new EA and DR rates are NOT subtle, as shown in Fig. 14. In this comparison the normalization is made to the central chord brightness of the Mo^{30+} line. Normalization to the Mo^{31+} line would yield discrepancies of a factor of $\sim$8 in the comparisons of the central chord brightnesses of the Mo^{29+}, and Mo^{25+} - Mo^{23+} lines. As is, the discrepancies are $\sim$3 for Mo^{31+} and Mo^{29+}, and a factor of about 2.5 for the other lines. Again, these differences are largely due to the absence of EA in the ionization rate coefficients.

It is clear from these profile observations that determination of a total molybdenum density from the central chord line brightness from a centrally peaked charge state will be sensitive to the accuracy of the ionization balance for that charge state. Errors in the ionization balance will not as greatly affect a molybdenum density determination from a charge state which peaks outside of the core, because even if it appears at a temperature different than predicted, the predictions still show it in its maximum fractional abundance at some temperature. For example, calibrating the molybdenum density to the non-central Mo^{29+} 122.42 Å line brightness in both Figs 13 and 14 results in a difference of only a factor of $\sim$20% in the deduced molybdenum density. However, as implied in the previous paragraph, the difference in the molybdenum density is over a factor of 4, when deduced using the old and new accurate ionization balance and when using the Mo^{31+} line. Of course measurements using a non-central charge state will not yield a determination of the *central* molybdenum concentration. Therefore, an accurate ionization balance calculation is crucial for an accurate central molybdenum concentration.

Conclusions

A systematic study of the atomic physics of emission from medium-to-high charge states of molybdenum has been performed by comparing the measured

brightness profiles of lines from eight ionization states with those predicted by a model which determines the ionization balance and impact excitation rates, uses the measured impurity transport coefficients and electron density and temperature profiles, and includes reconstruction of instrumental views through the plasma. In the calculation, excitation rate coefficients and level populations were calculated using the HULLAC package. The relative magnitudes of the excitation rate coefficients for the set of 2p-nd x-ray transitions in Mo^{32+} were shown to be consistent with the measured brightnesses, even reproducing the subtle effects which occur as a result of configuration mixing. The excitation rate coefficients for a large number of observed lines have been fit to a common analytic expression.

Initial quantitative comparisons of measured profiles with model predictions which included only direct ionization indicated that the charge state balance was not being correctly modeled. Calculations in Ref. 8 of the excitation-autoionization rate coefficients showed that this process was a significant ionization mechanism at least for the charge states Mo^{26+} through Mo^{31+}. Inclusion of these rate coefficients and of *ab initio* dielectronic recombination rate coefficients, calculated specifically for Mo^{25+} through Mo^{33+}, resulted in excellent agreement between the experimental profiles and those predicted. The improvement in the comparison is due primarily to the enhanced ionization rates brought about by EA. With this good agreement, accurate molybdenum concentration determinations can be made from brightness measurements of a single line. In fact, the determination of the molybdenum concentration in Alcator C-Mod appears now to be limited to the instrumental calibration uncertainties ($\sim$50%) rather than the model uncertainties.

The measurement of the spatial brightness profiles of lines from several centrally-peaked charge states does provide a reasonable test for predictions of the ionization balance.

Acknowledgements

The authors would like to thank J. Irby for electron density measurements,

S. Wolfe for flux surface reconstructions, H. Ohkawa for help with writing some of the computer codes used, and the ICRF and Alcator C-Mod operations groups for expert running of the tokamak. We also thank Princeton Plasma Physics Laboratory for the use of the MIST impurity transport code. Work supported at MIT by DoE Contract No. DE-AC02-78ET51013 and at LLNL by DoE Contract No. W-7405-ENG-48.

References

[1] D.E. Post, J of Nucl. Mater. **220-222**, 143 (1995)

[2] I.H.Hutchinson et al., Phys. Plasmas **1**, 1511 (1994)

[3] F. Alladio, et al., Plasma Physics and Controlled Fusion, **36**, B253 (1994)

[4] Phillips, V., et al, Plasma Physics and Controlled Nuclear Fusion, Seville (1994) 4-P-19

[5] Fussmann, G., et al, Plasma Physics and Controlled Nuclear Fusion, Seville (1994) A2-4-P-18

[6] D.H. Crandall, et al., Phys. Rev. A, **34** 1757 (1986)

[7] K.J. Reed, M. Chen, and D. Moores, Phys. Rev. A, **44** 4336 (1991)

[8] K. Fournier et al., submitted to Phys. Rev. A

[9] M. Chen, Phys. Rev. A, **38** 2332 (1988); M. Chen, Phys. Rev. A, **34** 1073 (1986).

[10] K.B. Fournier, W.H. Goldstein, D. Pacella, R. Bartiromo, M. Finkenthal, and M.J. May, accepted for publication in Phys. Rev. E (1995).

[11] R.A.Hulse, Nucl. Tech./Fus. **3**, 259 (1983). The authors thank PPPL for the use of the MIST code.

[12] J.E.Rice and E.S.Marmar, Rev. Sci. Instrum. **61**, 2753 (1990)

[13] M.A.Graf, Ph.D. Thesis, MIT (1995)

[14] Product sold by EG&G Reticon, Salem, MA

[15] L.L.Lao et al., Nucl. Fusion **25**, 1611 (1985)

[16] M.J. May, M. Finkenthal, S.P. Regan, H.W. Moos, J.L. Terry, M.A. Graf, K.B. Fournier, and W.L. Goldstein, Rev. Sci. Instrum. **66**, 561 (1995).

[17] S.N.Golovato, M. Porkolab, Y. Takase et al., in *Proceedings of the 11th Topical Conference on Radio-Frequency Power in Plasmas*, Palm Springs, CA (AIP, New York, 1995), (to be published).

[18] T.C.Hsu et al., Proc. 8th Joint Workshop on ECE and ECRH, IPP III/186, 409 (1993)

[19] J.H.Irby et al., Rev. Sci. Instrum. **59**, 1568 (1988)

[20] M.A.Graf et al., Rev. Sci. Instrum. **66**, 636 (1995)

[21] R.C.Isler, Nucl. Fusion **24**, 1599 (1984)

[22] D. Sampson and L. Golden, Ap. J., **170**, 169 (1971)

[23] D.E. Post, R.V. Jensen, C.B. Tarter, W.H. Grasberger, and W.A. Lokke, At. Data Nucl. Data Tables, **20**, 397 (1977)

[24] A.Burgess, Ap. J. **139**, 776 (1964)

[25] A.Burgess, Ap. J. **141**, 1588 (1965)

[26] A.Mertz et al., LASL Report LA-6220-MS (1976)

[27] J.E.Rice, et al., Phys. Rev. A **51**, 3551 (1995)

[28] Equipe TFR, Nucl. Fusion **15**, 1053 (1975)

[29] E.Hinnov, Phys. Rev. A **14**, 1533 (1976)

[30] M.W.D.Mansfield et al., J. Phys. B **11**, 1521 (1978)

[31] M.Finkenthal et al., J. Phys. B **18**, 4393 (1985)

[32] A.Wouters et al., J. Opt. Soc. Am. B **5**, 1520 (1988)

[33] J.Reader et al., J. Opt. Soc. Am. B **7**, 1176 (1990)

[34] J.Sugar et al., J. Opt. Soc. Am. B **6**, 1437 (1989)

[35] J.Sugar et al., J. Opt. Soc. Am. B **5**, 2183 (1988)

[36] V.Kaufman et al., J. Opt. Soc. Am. B **6**, 1444 (1989)

[37] J.Sugar et al., J. Opt. Soc. Am. B **4**, 1927 (1987)

[38] V.Kaufman et al., J. Opt. Soc. Am. B **6**, 142 (1989)

[39] P.Burkhalter et al., Phys. Rev. A **18**, 718 (1978)

[40] P.Burkhalter et al., J. Opt. Soc. Am. **67**, 1521 (1977)

[41] M.Klapisch, Comput. Phys. Commun. **2**, 269 (1971)

[42] M.Klapisch et al., J. Opt. Soc. Am. **67**, 148 (1977)

[43] A.Bar-Shalom et al., Phys. Rev. A **38**, 1773 (1988)

[44] R.Mewe, Astron. and Astrophys. **20**, 215 (1972)

[45] R.D.Cowan, The Theory of Atomic Structure and Spectra, University of California Press, pp.433-434 (1981)

Table Captions

Table I The x-ray and VUV lines, wavelengths and transition designations used for profile measurements. The upper states of the x-ray transitions are indicated by a series of jj-coupled orbitals; - represents l-s, while + represents l+s.

Table II X-ray and VUV lines for which excitation rates have been calculated. f_{ij} are the oscillator strengths and A and B are constants used in an empirical fit to the Gaunt factor (Eq. 3). The f_{ij}s for the $\Delta n \geq 1$ x-ray lines are from Ref. 27, while those for the $\Delta n = 0$ VUV lines were calulated using the CROSS codes.

Table I

Isosequence	Charge State	Wavelength (Å)	Transition
Fl	33+	3.6149[27]	$2p^5$ J=3/2 – $(2p_-)^2(2p_+)^2 4d_+$ J=5/2
			$2p^5$ J=3/2 – $(2p_-)^2(2p_+)^2 4d_+$ J=3/2
Ne	32+	3.6261[27]	$2p^6 - (2p_-)(2p_+)^4 4d_-$ J=1
		3.7398	$2p^6 - (2p_-)^2(2p_+)^3 4d_+$ J=1
Na	31+	3.6710[27]	$2p^6 3s - 2p_-[3s]4d_-$ J=1/2
			$2p^6 3s - 2p_-[3s]4d_-$ J=3/2
		3.7857[27]	$2p^6 3s - 2p_+[3s]4d_+$ J=3/2
		126.994[33]	$3p\ ^2P_{\frac{3}{2}} - 3d\ ^2D_{\frac{5}{2}}$
		127.873[33]	$3s\ ^2S_{\frac{1}{2}} - 3p\ ^2P_{\frac{3}{2}}$
Mg	30+	3.7155[27]	$2p^6 3s^2 - 2p_-[3s^2]4d_-$ J=1
		3.8348[27]	$2p^6 3s^2 - 2p_+[3s^2]4d_+$ J=1
		115.999[34]	$3s^2\ ^1S_0 - 3s3p\ ^1P_1$
Al	29+	122.420[35]	$3s^2 3p\ ^2P_{\frac{1}{2}} - 3s^2 3d\ ^2D_{\frac{3}{2}}$
Cl	25+	76.624[36]	$3p^5\ ^2P_{\frac{3}{2}} - 3p^4(^3P)3d\ ^2D_{\frac{5}{2}}$
Ar	24+	74.171[37]	$3p^6\ ^1S_0 - 3p^5 3d\ ^1P_1$
K	23+	70.596[38]	$3p^6 3d\ ^2D_{\frac{3}{2}} - 3p^5 3d^2(^3P)\ ^2P_{\frac{1}{2}}$
		70.726[38]	$3p^6 3d\ ^2D_{\frac{3}{2}} - 3p^5 3d^2(^3F)\ ^2D_{\frac{3}{2}}$
		71.175[38]	$3p^6 3d\ ^2D_{\frac{5}{2}} - 3p^5 3d^2(^3P)\ ^2P_{\frac{3}{2}}$
		72.050[38]	$3p^6 3d\ ^2D_{\frac{5}{2}} - 3p^5 3d^2(^3F)\ ^2P_{\frac{5}{2}}$

Table II

Charge State	Transition	Wavelength (Å)	f_{ij}	A	B
33+	2p-4d	3.6149	.267	.13	.097
32+	2p-4d	3.7398	.517	.090	.14
	2p-4d	3.6261	.302	.10	.10
	2p-5d	3.3920	.214	.14	.068
	2p-5d	3.2958	.111	.089	.11
	2p-6d	3.2301	.119	.11	.096
	2p-6d	3.1414	.0197	.060	.21
	2p-7d	3.1385	.113	.12	.075
	2p-7d	3.0549	.0381	.031	.15
	2p-8d	3.0831	.0511	.043	.13
	2p-8d	3.0007	.0108	.14	.11
	2p-9d	3.0456	.0344	.12	.079
	2p-9d	2.9664	.0242	-.09	.22
	2p-10d	3.0198	.0156	.00	.036
	2p-10d	2.9411	.00901	.22	.021
	2p-11d	3.0007	.0419	-.061	.20
	2p-11d	2.9228	.00940	.016	.18
	2p-12d	2.9864	.0140	.093	.097
	2p-12d	2.9102	.00745	.014	.16
31+	2p-4d	3.7857	.307	.15	.050
	2p-4d	3.6710	.225	.064	.12
	3s-3p	127.873	.201	.48	.33
30+	2p-4d	3.8348	.503	.11	.068
	2p-4d	3.7155	.286	.069	.11
	3s-3p	115.999	.529	.43	.38
29+	3p-3d	122.420	.115	.47	.34
25+	3p-3d	76.624	.695	.29	.48
24+	3p-3d	74.171	1.75	.31	.41
23+	3p-3d	70.596	.205	.29	.43
	3p-3d	70.726	.723	.28	.43
	3p-3d	71.175	.396	.29	.43
	3p-3d	72.050	.697	.30	.43

Figure Captions

Fig. 1 Flux surface reconstructions showing the scanning ranges of the VUV (dash-dot-dot-dot-dash) and x-ray (dashed) spectrometer systems. Also shown are surfaces of the molybdenum tile armor, the reconstructed magnetic equilibrium, two characteristic viewing lines-of-sight, and the mapping of those lines-of-sight to a midplane ρ.

Fig. 2 Time histories of several parameters of interest for a 5.4 T, deuterium ICRF heated discharge. Note the intentional injection of Mo at 0.4 s.

Fig. 3 Electron temperature (top) and density (bottom) spatial profiles at .65 s (solid curves) and .4 s during the Mo injection (dotted lines).

Fig. 4 Calculated molybdenum charge state radial profiles a.) with excitation-autoionization (EA) and new dielectronic recombination (DR) rates and b.) with old DR rates and without EA. Solid lines are for even charge states and dashed lines are for odd.

Fig. 5 The x-ray spectrum between 3.7 and 3.8 Å, showing 2p-4d transitions in the charge states Mo^{30+} through Mo^{33+}. Also visible are some argon and chlorine lines. a.) Near central chord spectrum, b.) predicted central chord spectrum for Ne-like (solid line), Na-like (dotted), Mg-like (dash-dot-dash) and F-like (dashed), and c.) spectrum taken along an off-axis chord, ρ=6.5 cm.

Fig. 6 The x-ray spectrum between 3.6 and 3.7 Å, showing 2p-4d transitions in Na-, Ne- and F-like molybdenum. a.) Near central chord spectrum, b.) the predicted central chord spectrum and c.) off-axis spectrum with ρ=6.7 cm.

Fig. 7 The VUV spectrum between 115 and 130 Å. a.) Near central chord spectrum, b.) predicted central chord Mo spectrum with the lines broadened to the instrumental resolution of the spectrograph, and c.) spectrum at ρ=7.4 cm. The actual equilibria and viewing chords are shown at the right.

Fig. 8 The VUV spectrum between 65 and 85 Å. a.) The measured near-central chord spectrum with identifications of known lines, b.) the spectrum shown in (a) with the unresolved "continuum" subtracted, and c) the predicted central chord Mo spectrum with individual lines shown and broadened to the spectrograph's instrumental resolution.

Fig. 9 Excitation rates as a function of electron temperature for the two 2p-nd series with $4 \leq n \leq 12$ of Mo^{32+}.

Fig. 10 Measured (symbols) and calculated (lines) brightnesses for the two 2p-nd series with $4 \leq n \leq 9$ of Mo^{32+} as a function of n.

Fig. 11 Measured (symbols) and calculated (lines) x-ray brightness profiles using the charge state density profiles of Fig. 4a. The solid lines are from Ne-like molybdenum, dotted lines from Na-like and dashed lines from F-like.

Fig. 12 Measured (symbols) and calculated (lines) x-ray brightness profiles, using the charge state density profiles of Fig. 4b.

Fig. 13 Measured (symbols) and calculated (lines) VUV brightness profiles for Na-like, Mg-like, and Al-like Mo lines (a), and for Cl-like, Ar-like and K-like Mo lines (b) using charge state density profiles which include EA and DR.

Fig. 14 Measured (symbols) and calculated (lines) VUV brightness profiles for Na-like, Mg-like, and Al-like Mo lines (a), and for Cl-like, Ar-like and K-like Mo lines (b) using charge state density profiles which do NOT include EA and DR.

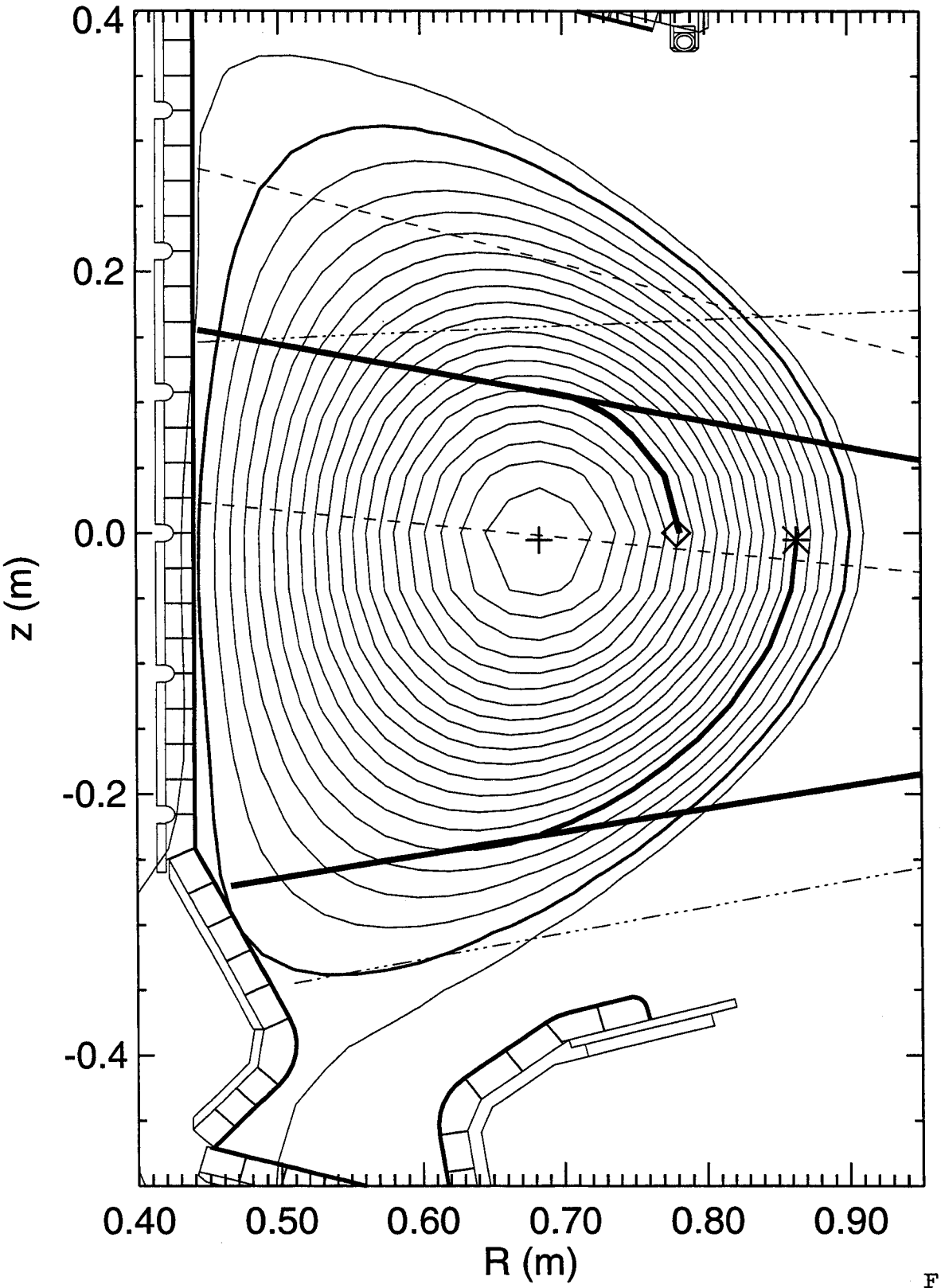

Figure 1

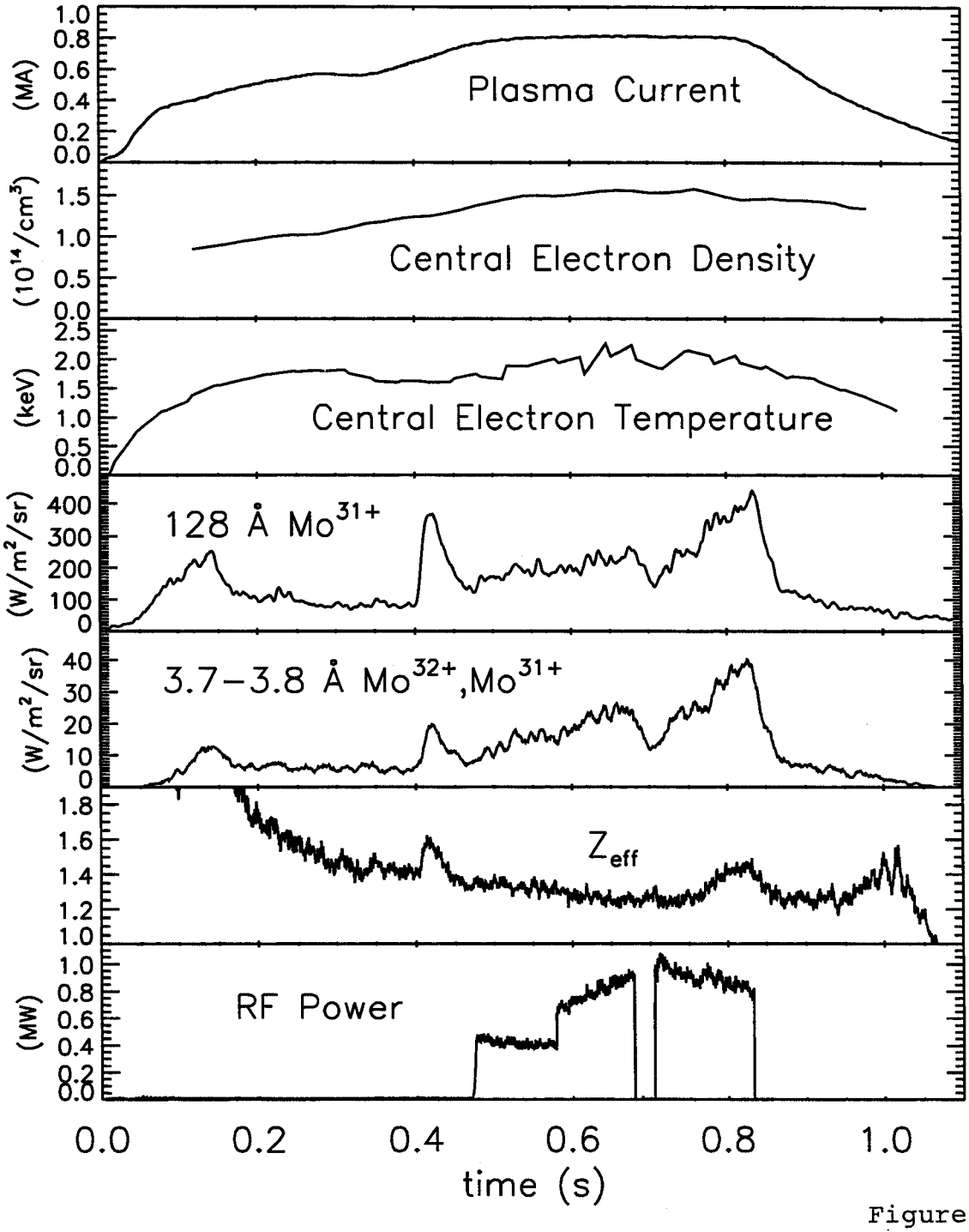
Plasma Current
(MA)
Central Electron Density
(10^14/cm^3)
Central Electron Temperature
(keV)
128 Å Mo^31+
(W/m^2/sr)
3.7–3.8 Å Mo^32+,Mo^31+
(W/m^2/sr)
Z_eff
RF Power
(MW)
time (s)

Figure 2

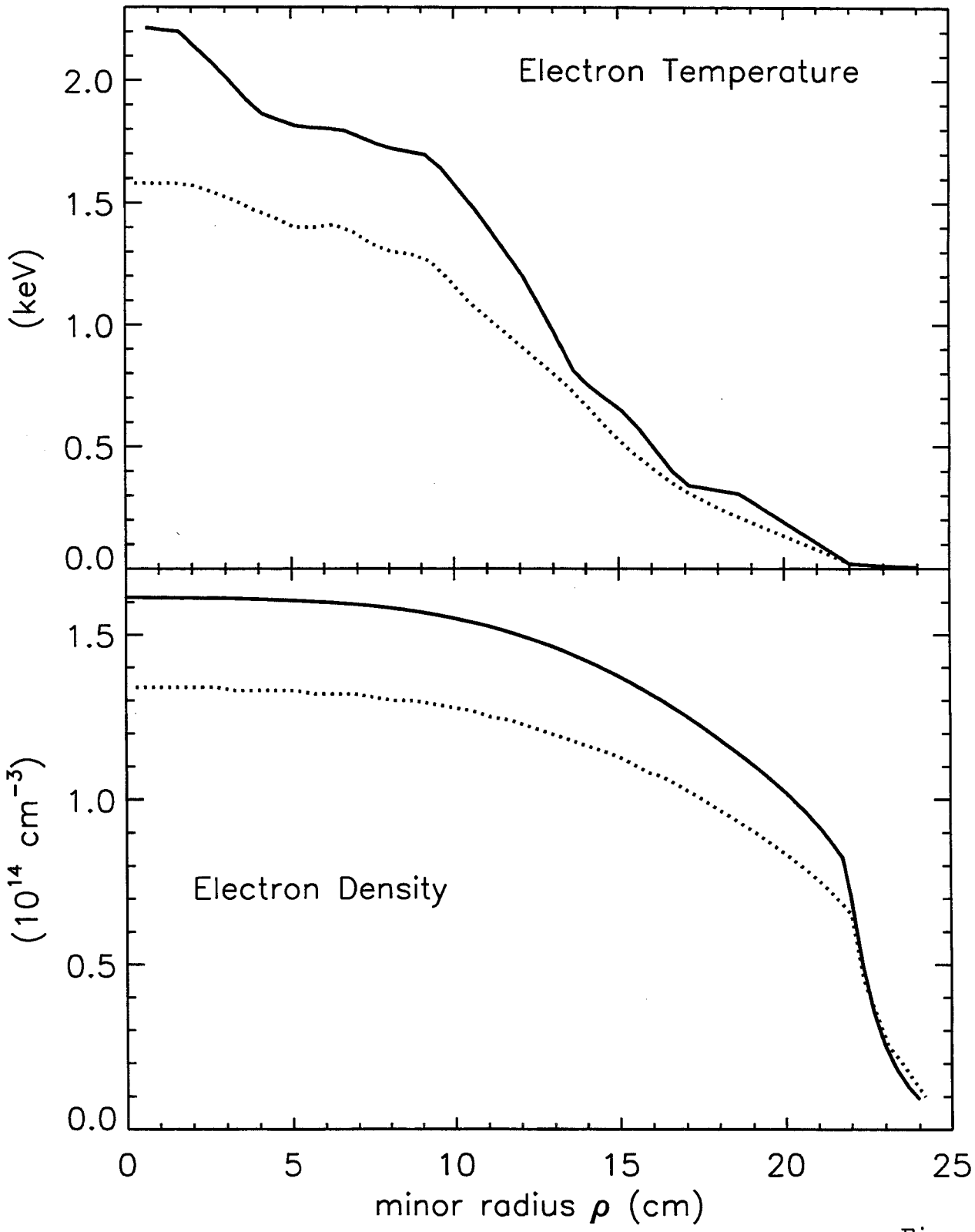
Electron Temperature
(keV)
2.0
1.5
1.0
0.5
0.0
Electron Density
$(10^{14}\ cm^{-3})$
1.5
1.0
0.5
0.0
0
5
10
15
20
25
minor radius ρ (cm)

Figure 3

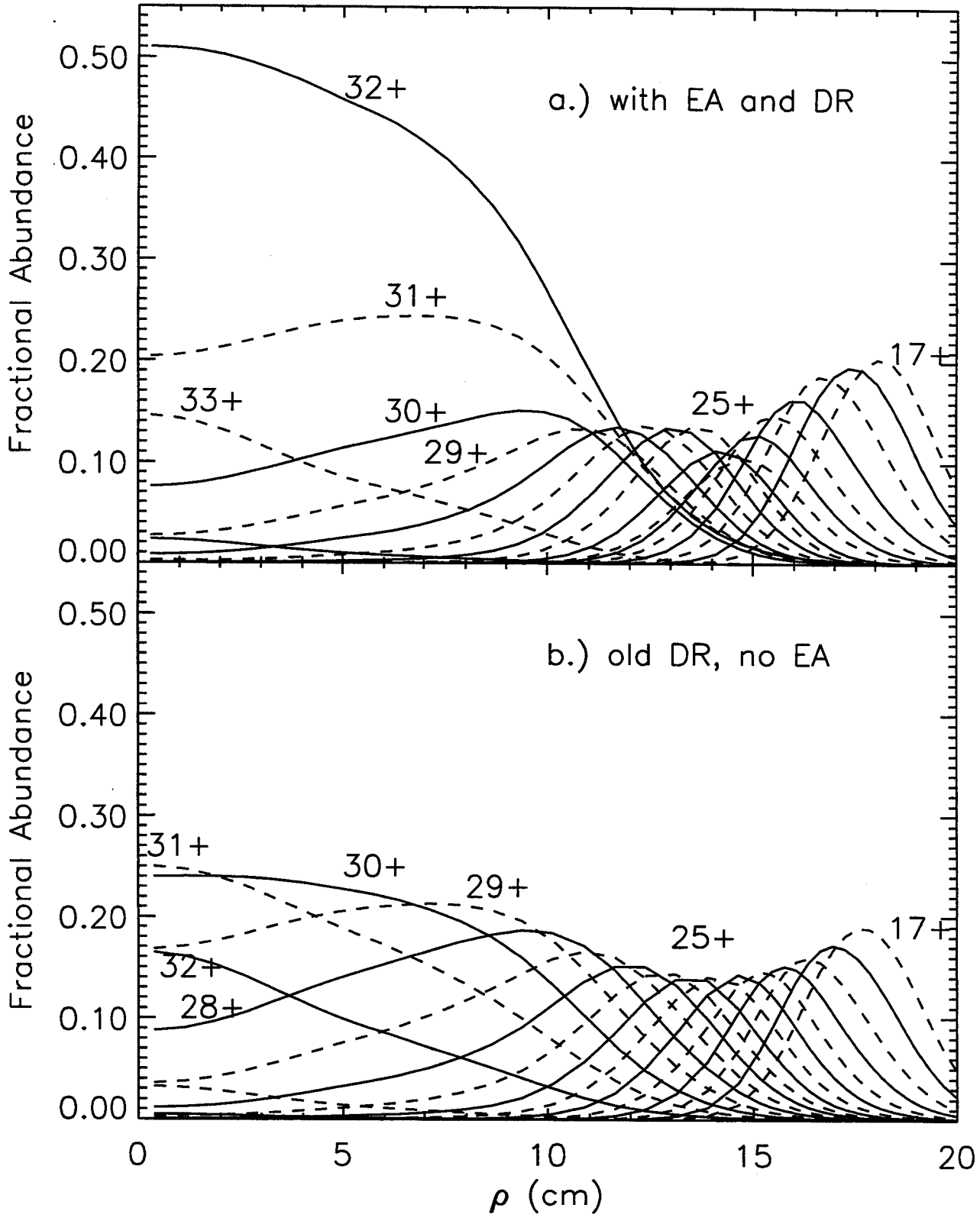
a.) with EA and DR
b.) old DR, no EA
Fractional Abundance
0.50
0.40
0.30
0.20
0.10
0.00
32+
31+
33+
30+
29+
25+
17+
28+
0
5
10
15
20
ρ (cm)

Figure 4

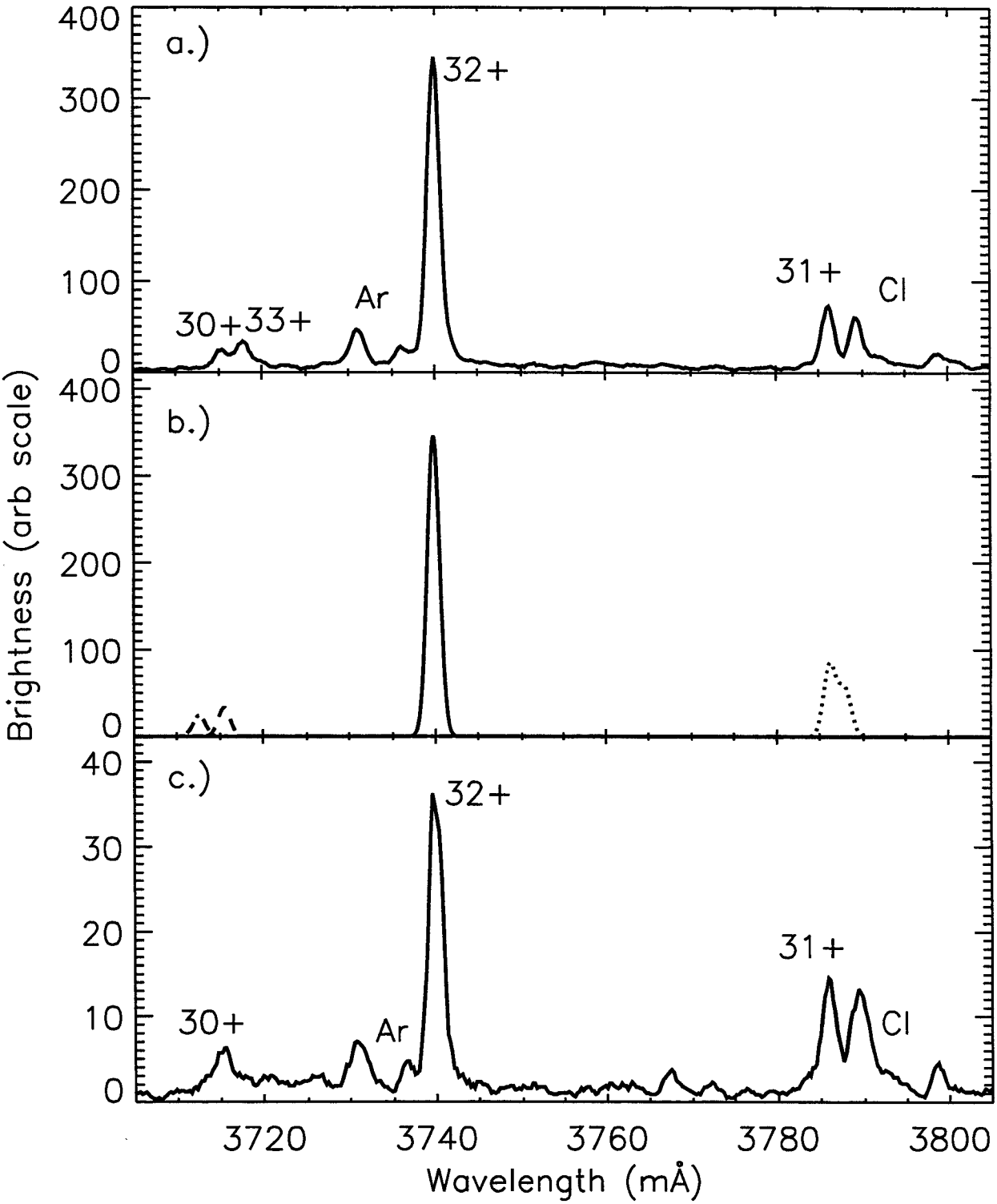
a.)
32+
31+
Cl
Ar
30+33+
b.)
c.)
32+
31+
30+
Ar
Cl
Brightness (arb scale)
Wavelength (mÅ)
3720
3740
3760
3780
3800

Figure 5

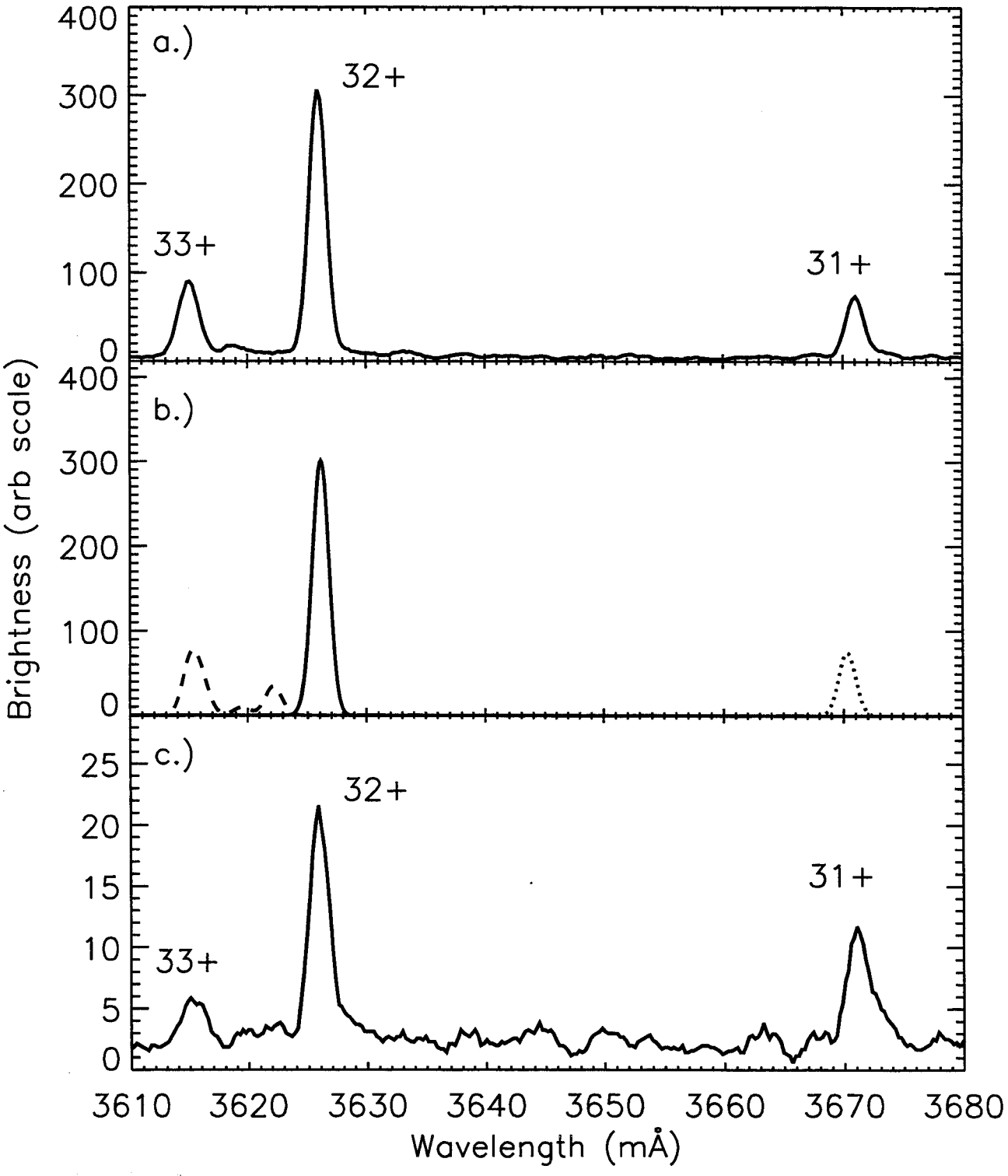
a.)
32+
33+
31+
b.)
c.)
32+
31+
33+
Brightness (arb scale)
Wavelength (mÅ)
400
300
200
100
0
25
20
15
10
5
3610
3620
3630
3640
3650
3660
3670
3680

Figure 6

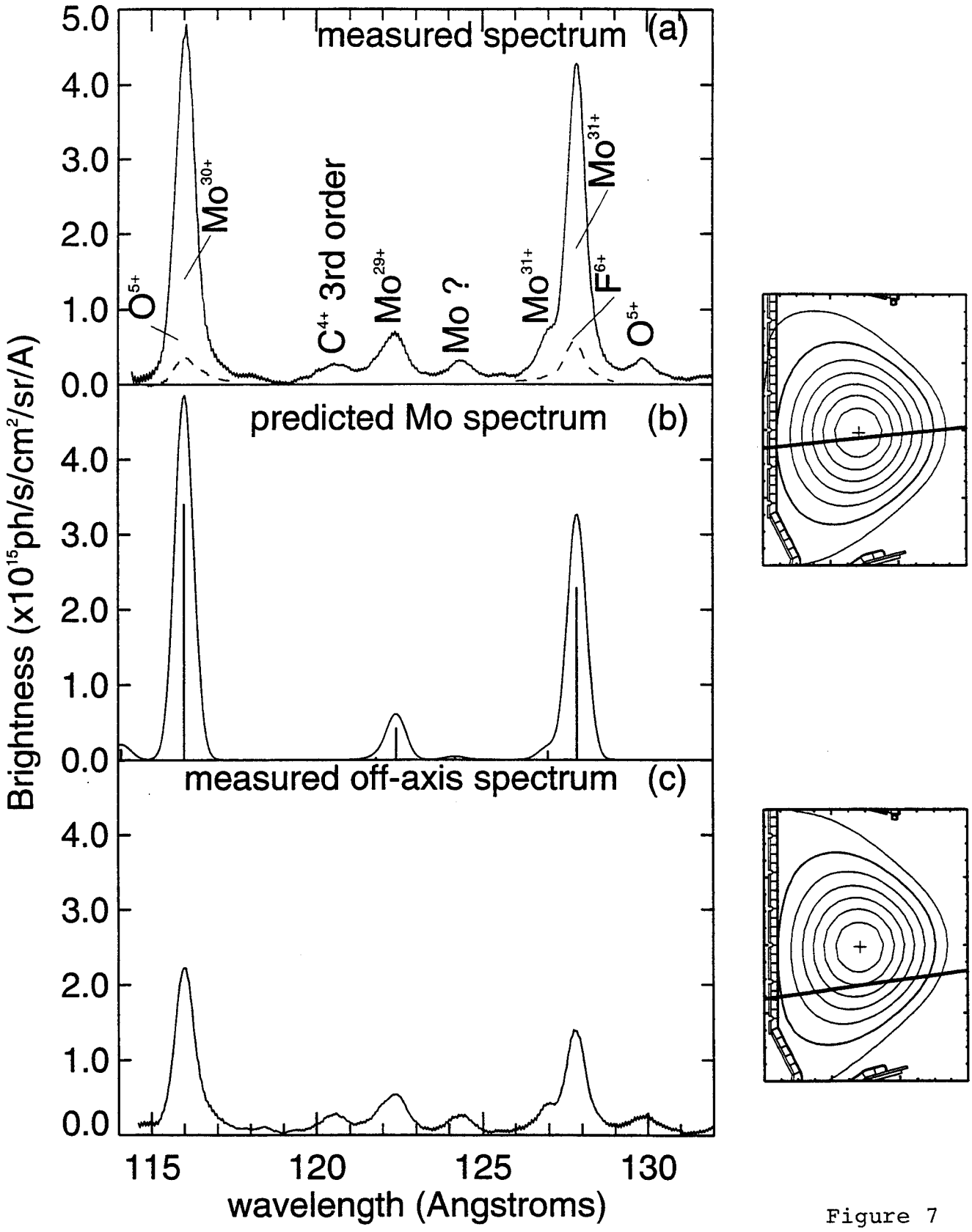
measured spectrum (a)
predicted Mo spectrum (b)
measured off-axis spectrum (c)
O5+
Mo30+
C4+ 3rd order
Mo29+
Mo ?
Mo31+
F6+
Mo31+
O5+
Brightness (x10^15 ph/s/cm^2/sr/A)
wavelength (Angstroms)
5.0
4.0
3.0
2.0
1.0
0.0
115
120
125
130

Figure 7

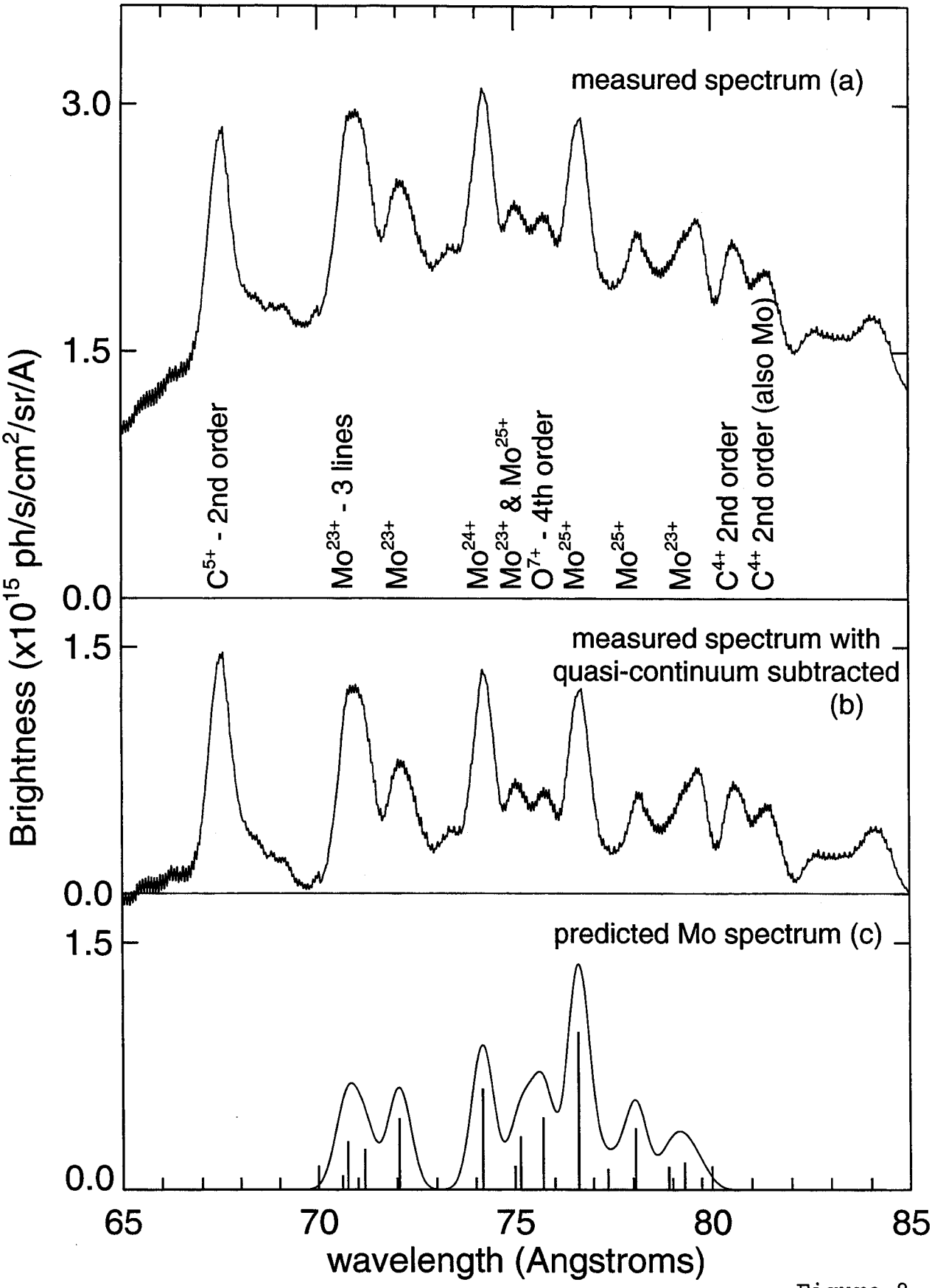
measured spectrum (a)
3.0
1.5
0.0
Brightness (x10^15 ph/s/cm^2/sr/A)
C5+ - 2nd order
Mo23+ - 3 lines
Mo23+
Mo24+
Mo23+ & Mo25+
O7+ - 4th order
Mo25+
Mo25+
Mo23+
C4+ 2nd order
C4+ 2nd order (also Mo)
measured spectrum with quasi-continuum subtracted (b)
1.5
0.0
predicted Mo spectrum (c)
1.5
0.0
65
70
75
80
85
wavelength (Angstroms)

Figure 8

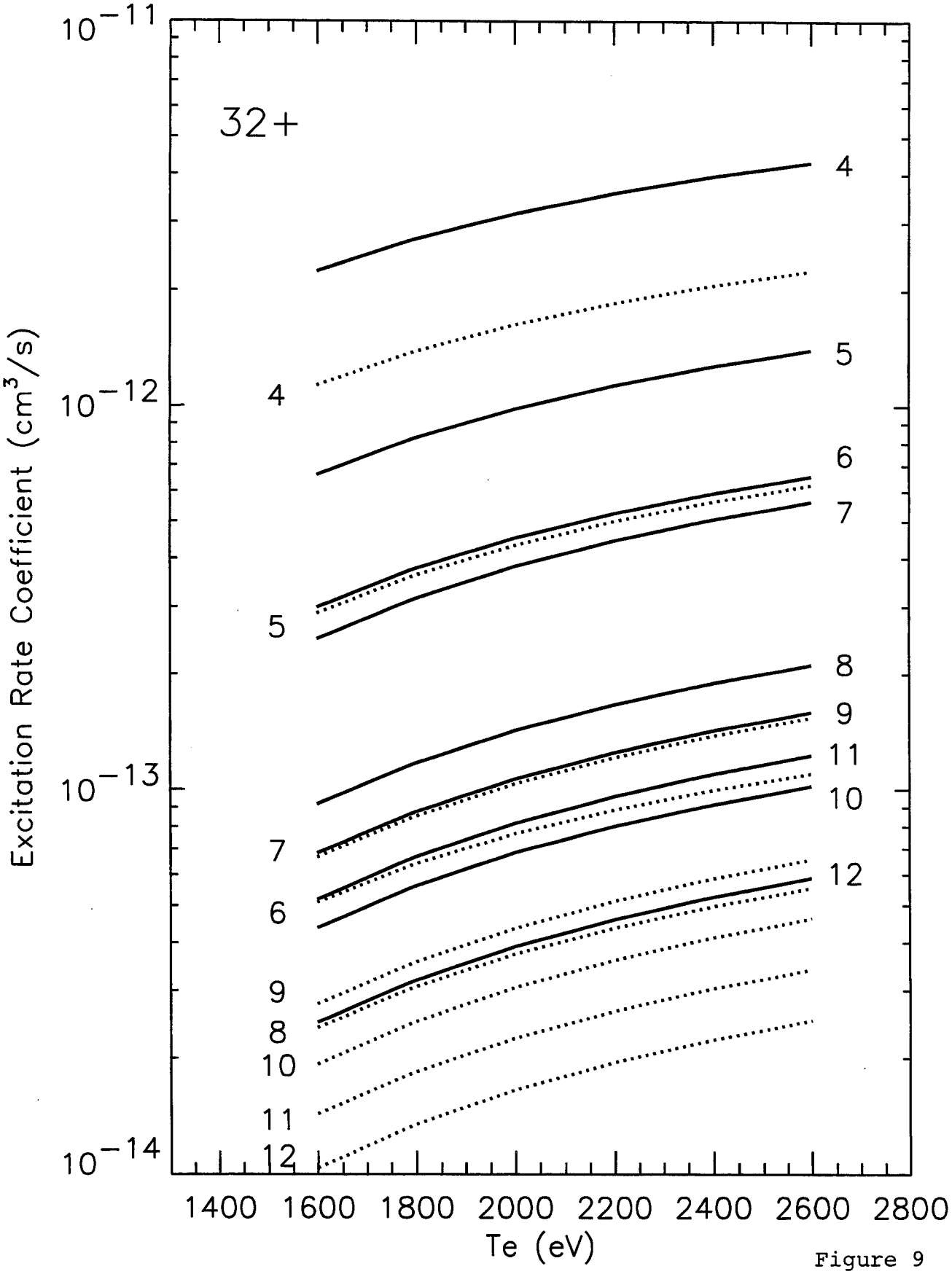
32+
Excitation Rate Coefficient (cm³/s)
10⁻¹¹
10⁻¹²
10⁻¹³
10⁻¹⁴
1400 1600 1800 2000 2200 2400 2600 2800
Te (eV)
4
5
6
7
8
9
11
10
12

Figure 9

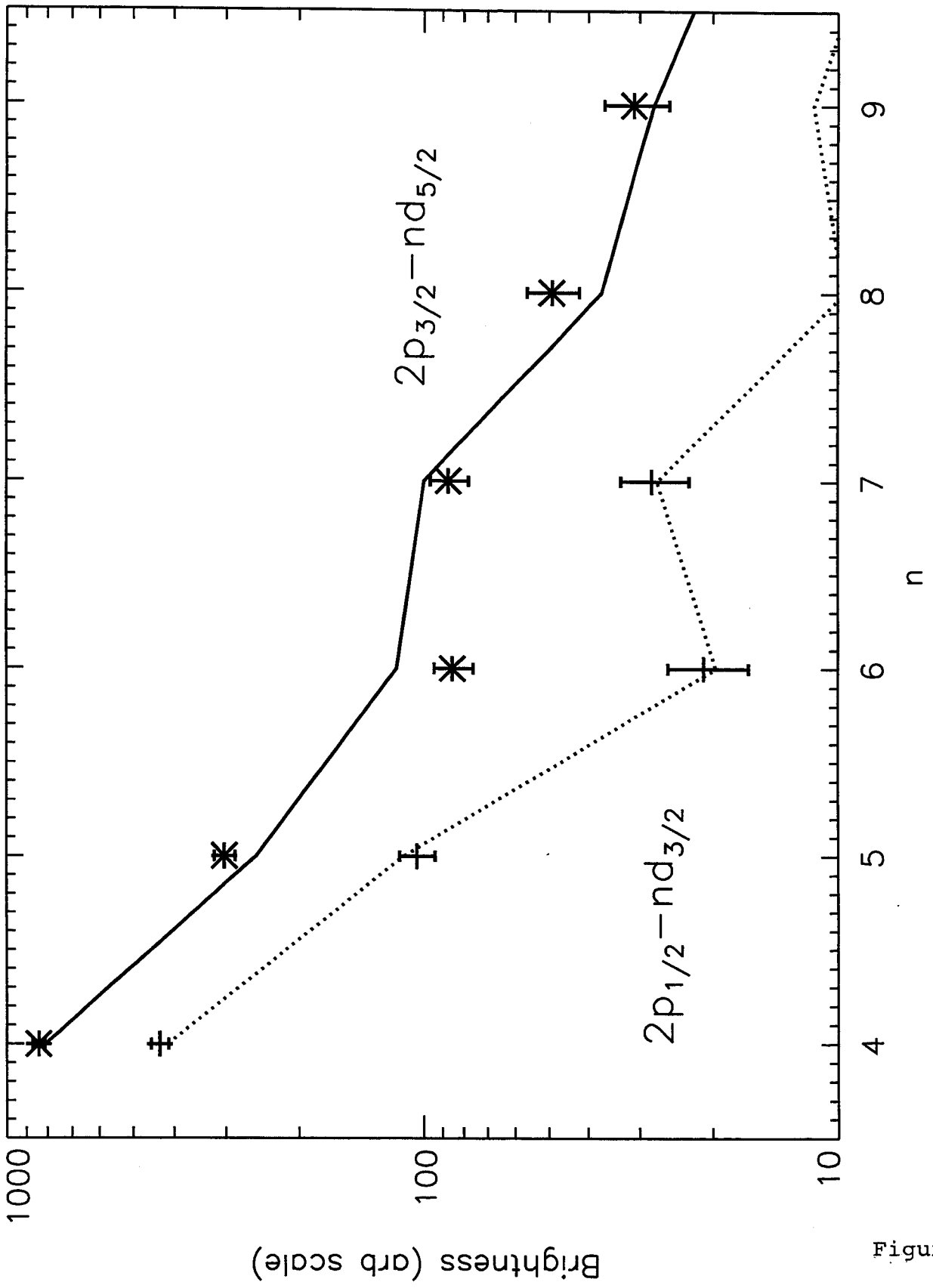
Brightness (arb scale)
1000
100
10
4
5
6
7
8
9
n
$2p_{3/2}-nd_{5/2}$
$2p_{1/2}-nd_{3/2}$

Figure 10

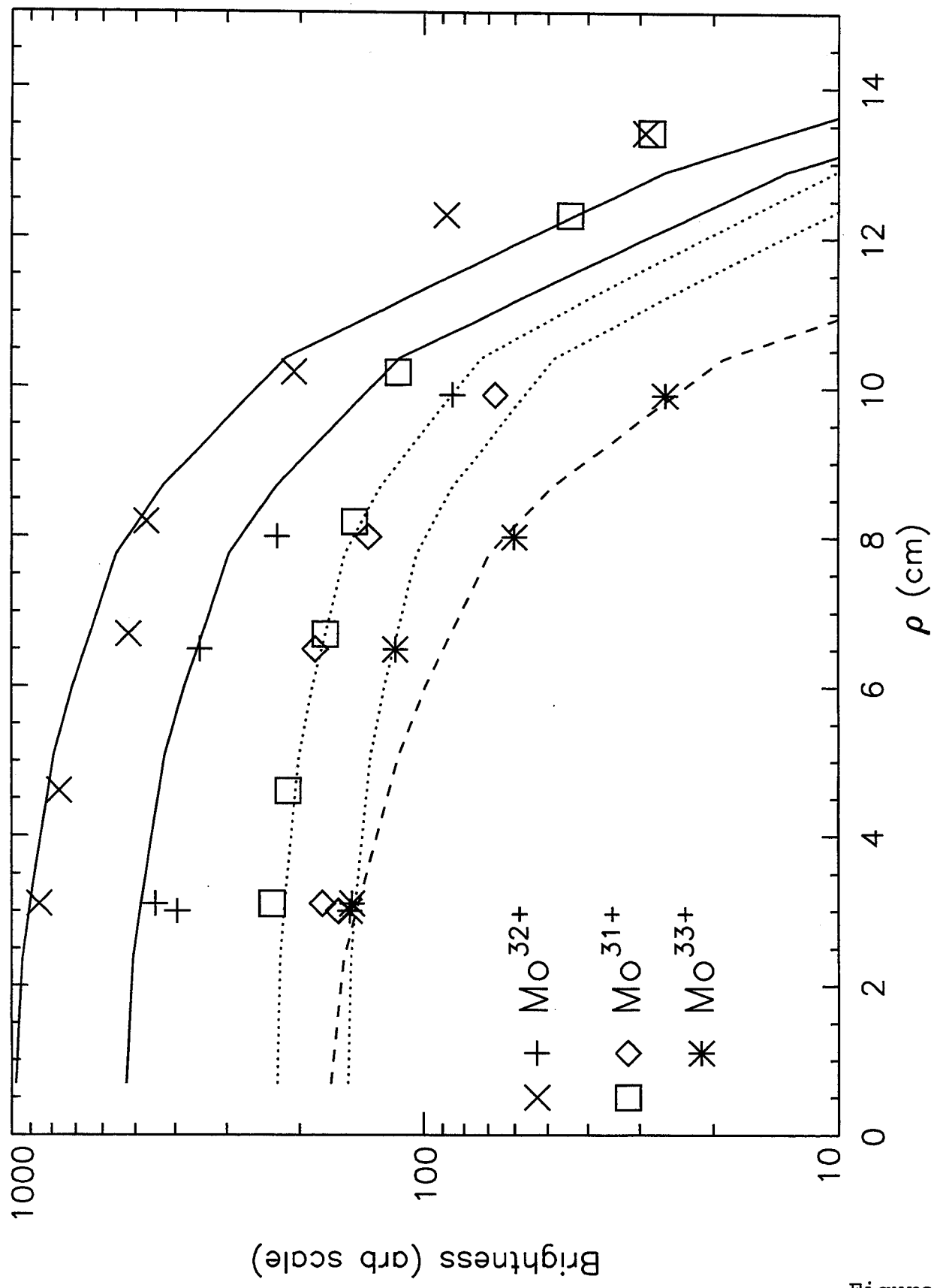
Brightness (arb scale)
1000
100
10
0
2
4
6
8
10
12
14
ρ (cm)
Mo32+
Mo31+
Mo33+

Figure 11

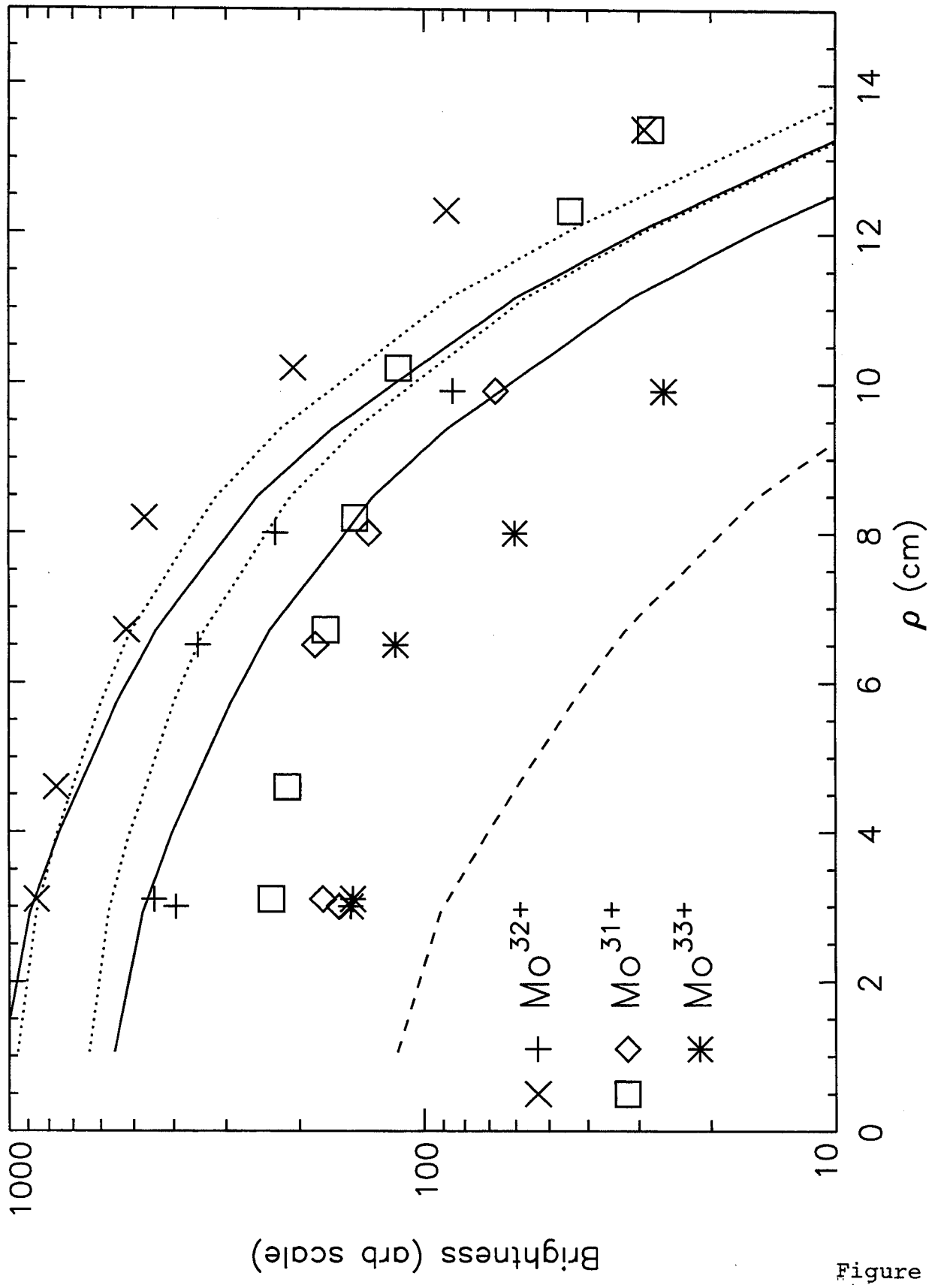
Brightness (arb scale)
1000
100
10
0
2
4
6
8
10
12
14
ρ (cm)
Mo32+
Mo31+
Mo33+

Figure 12

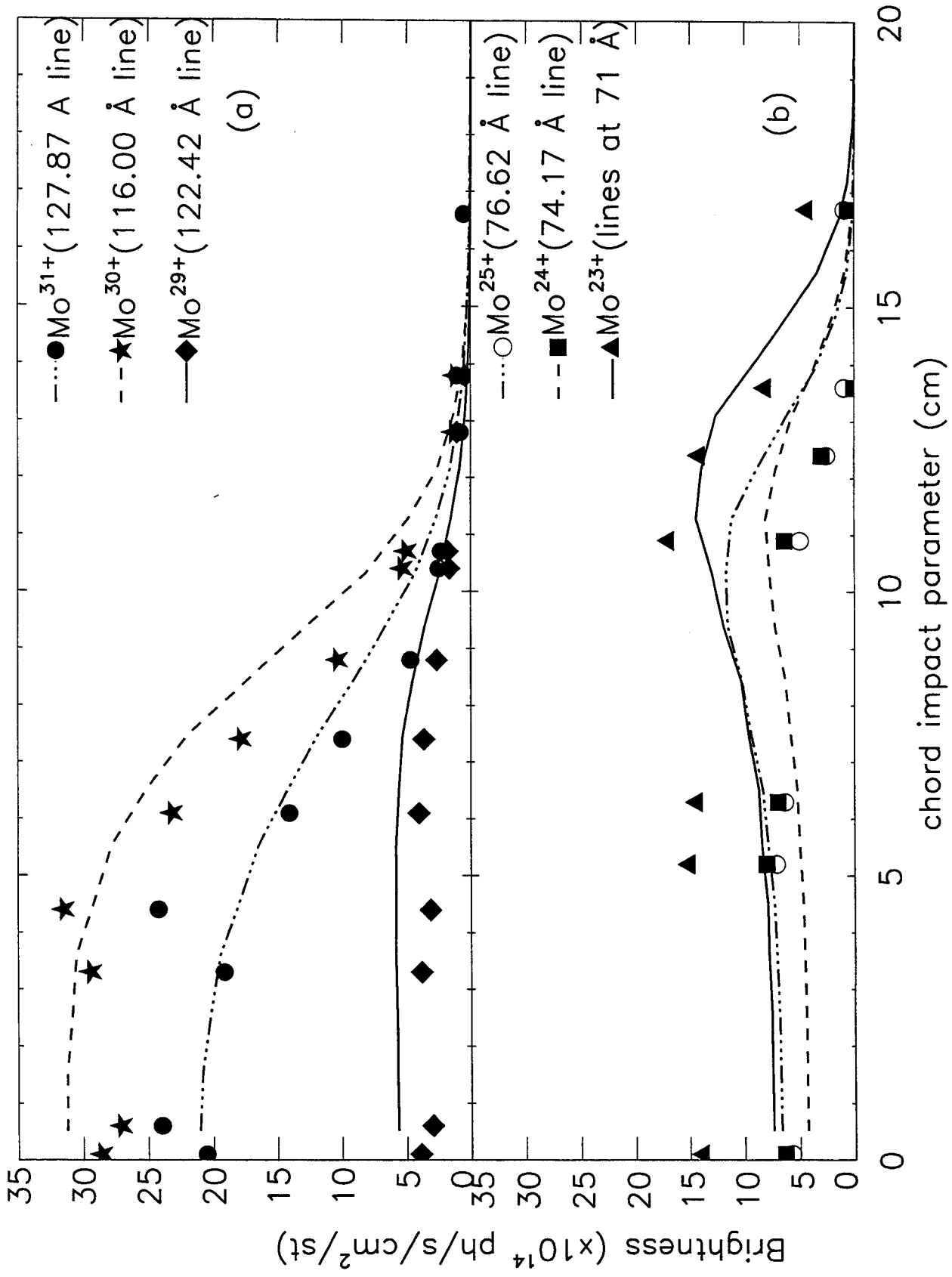
Mo31+(127.87 A line)
Mo30+(116.00 Å line)
Mo29+(122.42 Å line)
(a)
Mo25+(76.62 Å line)
Mo24+(74.17 Å line)
Mo23+(lines at 71 Å)
(b)
Brightness (x10^14 ph/s/cm^2/st)
chord impact parameter (cm)
0
5
10
15
20
25
30
35

Figure 13

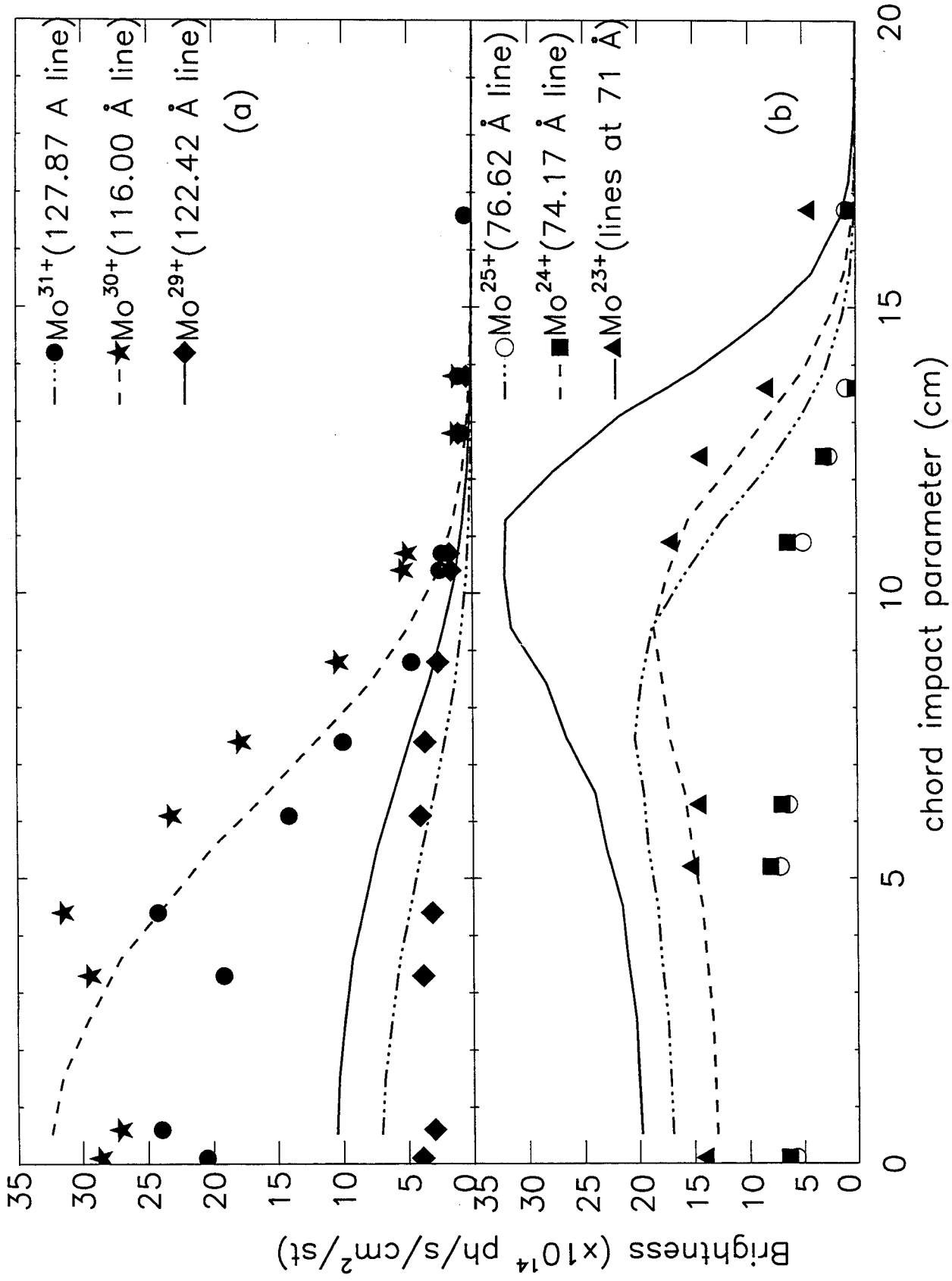
Mo31+(127.87 A line)
Mo30+(116.00 Å line)
Mo29+(122.42 Å line)
(a)
Mo25+(76.62 Å line)
Mo24+(74.17 Å line)
Mo23+(lines at 71 Å)
(b)
Brightness (x10^14 ph/s/cm^2/st)
chord impact parameter (cm)

Figure 14